Role of channel and floodplain cross-section geometry in the basin response

A. I. Mejia[1] and S. M. Reed[1]

Received 3 January 2011; revised 26 May 2011; accepted 15 July 2011; published 20 September 2011.

[1] We investigate the role of cross-section geometry in flow routing by developing an analytical framework based on the instantaneous response function (IRF) and relationships of river basin geomorphology. The cross-section geometry is included explicitly within the framework by assuming a power law cross section that is, in turn, used to derive expressions for the at-a-site hydraulic geometry. The analysis performed using the Illinois River basin indicates that the cross-section geometry takes on different roles depending on whether flows are in the channel or floodplain. The cross-section geometry where width dominates over depth (width dominant), i.e., the at-a-site width-depth ratio increases with increasing depth, tends to produce a larger network celerity and dispersion for the channel, and the trend reverses for the high floodplain flows. We found that the cross-section geometry can influence the relative contribution of hydrodynamic and kinematic dispersion. For the channel, the depth-dominant cross section produces a lower hydrodynamic dispersion than the width-dominant cross section and vice versa for the floodplain. We found that the nonlinear dependence of the IRF on effective rainfall, expressed in the IRF time to peak and peak flow, may vary depending on the cross-section geometry, with the nonlinearity decreasing for the width-dominant cross sections. Additionally, the effect of cross-section geometry on the basin response can alter the relative contribution of the stream network and hillslopes to the basin dispersion. The derived framework has potential as an a priori tool for incorporating channel and floodplain geometry into distributed rainfall-runoff models.

Citation: Mejia, A. I., and S. M. Reed (2011), Role of channel and floodplain cross-section geometry in the basin response, *Water Resour. Res., 47*, W09518, doi:10.1029/2010WR010375.

1. Introduction

[2] In stream networks, there exists a close relationship between cross-section form and river flows. This connection can result in a high degree of temporal and spatial regularity as expressed in the at-a-site and downstream hydraulic geometry relationships, respectively, of *Leopold and Maddock* [1953]. This is the case despite the cross-section geometry being shaped and influenced, in a dynamic and complex stream network system, by fluvial processes and interacting factors (i.e., streamflows, sediments, vegetation, and cross-section characteristics) [*Leopold and Maddock*, 1953; *Schumm*, 1960; *Wilcock*, 1971; *Miller and Onesti*, 1979; *Miller*, 1984; *Western et al.*, 1997; *Gregory*, 2006; *Muneepeerakul et al.*, 2007]. In this study we mean by cross-section geometry the approximate shape of a cross section (e.g., parabolic, triangular, etc.), while hydraulic geometry refers exclusively to the power law relationships between cross-section properties and river flows [*Leopold and Maddock*, 1953]. Hydraulic geometry relationships have been used to investigate the instantaneous response function (IRF) of the network and basin and the response nonlinearity [*Robinson et al.*, 1995; *Saco and Kumar*, 2002a, 2002b, 2004; *Paik and Kumar*, 2004]. We expand and complement these previous investigations by accounting for the role of both channel and floodplain cross-section geometry.

[3] *Saco and Kumar* [2002a, 2002b] showed that hydraulic geometry may be incorporated into the geomorphologic response function, following the pioneering work of *Rinaldo et al.* [1991] on geomorphic dispersion and of *Rodriguez-Iturbe and Valdés* [1979] on the geomorphologic instantaneous unit hydrograph (IUH), and that it can produce an additional so-called kinematic dispersion effect. *Paik and Kumar* [2004] found that hydraulic geometry can influence the nonlinearity of the network response. These investigations indicate that both hydraulic and stream network geometry can shape the response at a shorter event time scale [*Saco and Kumar*, 2002a, 2002b, 2004; *Paik and Kumar*, 2004]. At longer time scales associated with channel and floodplain formation, expressed by a wide range of frequencies of discharge, *Dodov and Foufoula-Georgiou* [2005] found streamflow variability to influence hydraulic geometry and vice versa. Indeed, the influence of hydraulic geometry on the network response function was present implicitly in the early theory of the geomorphoclimatic IUH through the kinematic wave exponent [*Rodriguez-Iturbe et al.*, 1982]. In the geomorphoclimatic IUH the explicit assumption was made of a rectangular cross-section shape [*Rodriguez-Iturbe et al.*, 1982]. Similarly, the nonlinear IUH formulation of *Wang et al.* [1981] implied a

[1]Office of Hydrologic Development, National Weather Service, NOAA, Silver Spring, Maryland, USA.

Copyright 2011 by the American Geophysical Union.
0043-1397/11/2010WR010375

wide rectangular cross section. This assumption can have important effects on hydrograph simulation [*Orlandini and Rosso*, 1998]. The implications of this assumption are explored in this study from a more general approach. We use analytical expressions for the at-a-site hydraulic geometry that account explicitly for the cross-section form. With this we also seek to explain further the interdependence between hydraulic geometry and response nonlinearity [*Paik and Kumar*, 2004].

[4] In addition to the cross-section geometry influencing the response, it plays an important role in transport processes, riparian dynamics through the floodplain form, and practical applications, such as stream restoration, flood mapping, and discharge estimation from remote sensing [*Singh*, 1996; *Western et al.*, 1997; *Nardi et al.*, 2006; *Muneepeerakul et al.*, 2007; *Smith and Pavelsky*, 2008]. It is also used often as a proxy to quantify the effects of land use change from urbanization on streams [*Hammer*, 1972; *Leopold et al.*, 2005; *Gregory*, 2006]. Another area where cross-section geometry is of particular importance is in distributed rainfall-runoff and/or hydraulic modeling [*Fread*, 1993; *Orlandini and Rosso*, 1998; *Orlandini*, 2002; *Koren et al.*, 2004; *Camporese et al.*, 2010]. For example, the distributed model employed by NOAA's National Weather Service [*Koren et al.*, 2004], HL-RDHM, for operational forecasting assumes a power law cross section. It is often necessary in distributed models to make assumptions about the cross-section geometry when routing flows [*Fread*, 1993; *Orlandini and Rosso*, 1998; *Orlandini*, 2002; *Koren et al.*, 2004] because of a lack of cross-sectional data at all model nodes. Even with the availability of digital elevation models (DEMs), assumptions are necessary because the resolution of the DEM may not always be sufficient to resolve the main channel form and data used to derive DEMs do not often include channel bathymetry for perennial streams [*Dodov and Foufoula-Georgiou*, 2005; *Nardi et al.*, 2006]. Thus, part of the motivation behind this investigation is to help guide the development of routing parameterizations for distributed rainfall-runoff and/or hydraulic models with sparse data. To get to this point, we first use the IRF as a tool to characterize the impacts of parameterized cross-section shapes on flow routing. Other studies have looked at the role of cross-section geometry but not from the perspective of the stream network and the IRF [*Fread and Lewis*, 1986; *Garbrecht*, 1990; *Myers*, 1991; *Ponce and Porras*, 1995; *Valiani and Caleffi*, 2009]. The framework proposed in this study is novel in that it synthesizes at the basin scale the role of both channel and floodplain cross-section geometry in the hydrologic response. Further, this is achieved by utilizing in a novel way basin-wide patterns of hydrogeomorphic regularity as reflected in scaling relationships of fluvial geomorphology.

[5] This paper is organized as follows. In section 2, an analytical power law model of cross-section geometry is described and used to derive at-a-site hydraulic geometry relationships. In section 3, the cross-section geometry is included in the IRF using the derived at-a-site hydraulic geometry. Section 4 describes the data and conditions for a case study application. Using the case study, in section 5, we examine the effects of cross-section geometry on the network response, the response nonlinearity, and the basin dispersion. Last, the conclusions are summarized in section 6.

2. Model of Cross-Section and At-a-Site Hydraulic Geometry

2.1. Cross-Section Geometry

[6] To represent both channel and floodplain cross-section geometry, we assume power law cross sections [*Henderson*, 1966; *Fread and Lewis*, 1986; *Garbrecht*, 1990; *Koren et al.*, 2004; *Valiani and Caleffi*, 2009]. The advantage of the power law cross section is that it allows the consideration of various cross-section forms, it has been shown to be applicable to various hydrologic conditions, and it is analytically amenable [*Fread and Lewis*, 1986; *Garbrecht*, 1990; *Koren et al.*, 2004; *Valiani and Caleffi*, 2009].

[7] For the channel (i.e., below bankfull conditions), the power law cross section, for $h = 0$ at the cross-section bottom, $\beta \geq 0$, and $\alpha > 0$, is defined as follows:

$$W = \alpha h^{\beta}, \quad 0 \leq h \leq h_{\mathrm{bf}}. \tag{1}$$

W [L] is the cross-section width at a depth h [L], α [$L^{1-\beta}$] is the power law coefficient, β is the power law exponent that controls the shape of the cross section, and h_{bf} is the depth at bankfull. The subscript bf is used to denote bankfull conditions. When $\beta = 0$, the cross-section shape is rectangular. For the range $0 < \beta < 1$, the cross-section shape is parabolic. For $\beta = 1$ the shape is triangular. For $\beta > 1$, the width of the cross section increases nonlinearly with depth, resulting in an expanding V-shaped form. We will also refer to β as the cross-section shape factor. The power law in (1) assumes the cross-section shape to be symmetric.

[8] We also use the power law cross section in (1) to characterize the floodplain geometry where [*Garbrecht*, 1990]

$$W_f = W_{\mathrm{bf}}\left(\frac{\alpha_f}{W_{\mathrm{bf}}} h_f^{\beta_f} + 1\right) \tag{2}$$

and $h_f = 0$ at bankfull level. The subscript f denotes a floodplain value. W_{bf} is the cross-section width at bankfull. The remainder terms in (2) have the same meaning as in (1) but are defined for the floodplain only. The applicability of the power laws (1) and (2) to river cross sections has been demonstrated previously [e.g., *Fread and Lewis*, 1986; *Garbrecht*, 1990; *Jowett*, 1998; *Dingman*, 2007]. For example, *Fread and Lewis* [1986] used a separate power law relationship for the channel and floodplain exactly as we do here.

[9] By integrating (1) over dh, we obtain the following expression for the channel cross-sectional area A [L^2]:

$$A = \frac{\alpha}{(\beta + 1)} h^{\beta+1}. \tag{3}$$

On the basis of (2), the cross-sectional area for the floodplain A_f [L^2] is then defined as follows [*Garbrecht*, 1990]:

$$A_f = W_{\mathrm{bf}} h_f \left[\frac{\alpha_f}{W_{\mathrm{bf}}(\beta_f + 1)} h_f^{\beta_f} + 1\right]. \tag{4}$$

Additionally, we define the hydraulic depth H [L] as the ratio of A to W. From (1) and (3), H is then equal to $h/(1+\beta)$. Figure 1 illustrates the power law cross section and the role of β. It shows how the width-depth ratio W/H varies as a function of depth for various cross-section shape factors. A reasonable range for W/H in natural alluvial stream channels is between 1 and 100 [*Osterkamp et al.*, 1983]. Two distinct cross-section geometry groups can be identified in Figure 1, which will help us with our discussion later on. In the first group, bounded by the range $0 < \beta < 1$, the depth dominates over the width (i.e., W/H decreases with increasing depth). The cross-section shapes in this range are referred to as depth dominant. In the second group, defined by $\beta > 1$, the opposite is true; the width increases faster than the depth. These cross-sections shapes are referred to as width dominant. The value $\beta = 1$, where the width and depth are equally dominant, separates the two cross-section shape groups. The physical interpretation of these groups is given in terms of the sediment composition of the channel [*Leopold and Maddock*, 1953; *Schumm*, 1960; *Osterkamp et al.*, 1983; *Rhoads*, 1991; *Kolberg and Howard*, 1995]. The depth-dominant cross sections tend to be formed by finer, more cohesive material, and the width-dominant cross sections tend to have a greater proportion of sand material.

2.2. At-a-Site Hydraulic Geometry

[10] Equations (1) and (3) in combination with the Manning and continuity equation are used to derive analytical at-a-site hydraulic geometry expressions (see Appendix A for details). The at-a-site hydraulic geometry expressions are

$$W = a'Q^{b'}, \tag{5}$$

$$H = c'Q^{f'}, \tag{6}$$

$$V = k'Q^{m'}. \tag{7}$$

W [L], H [L], and V [$L\ T^{-1}$] are the water surface top width, mean water depth, and mean velocity, respectively. Q [$L^3\ T^{-1}$] is the cross-section discharge. Expressions (5), (6), and (7) correspond to (A3), (A2), and (A4), respectively, in Appendix A. To derive an at-a-site expression for the cross-section area A, (5) and (6) can be multiplied. Expressions (5)–(7) account for the cross-section geometry implicitly through the coefficient terms (i.e., a', c', and k'), which are dependent on α and β from (1), and the exponents (i.e., b',f', and m'), which are dependent on β.

[11] Similar expressions to (5)–(7) were previously derived by *Dingman* [2007] using a slightly different form for (1). We extend these expressions here to include the dependency of the hydraulic geometry coefficients on scale by expressing α, the channel bed slope s_o, and the channel roughness coefficient n as a function of drainage area (see Appendix A for the relationships between the at-a-site coefficients and α, s_o, and n). The actual scale-dependent expressions for α, s_o, and n are included in Appendix B1.

[12] For the floodplain geometry, to understand its separate effects and allow for analytical tractability, we make the simplifying assumptions that the channel and floodplain cross sections act as a single unit [*Bhowmik and Demissie*, 1982; *Buehler*, 1983; *Bhowmik*, 1984; *Woltemade and Potter*, 1994] and that the floodplain cross-sectional area is much larger than the bankfull area [*Fread and Lewis*, 1986]. These assumptions may be reasonable for larger flows, say larger than a 50 year return period [*Bhowmik and Demissie*, 1982; *Buehler*, 1983; *Bhowmik*, 1984; *Woltemade and Potter*, 1994], when the floodplain cross section is dominant [*Myers*, 1987] and the channel-floodplain interactions are minor [*Knight and Demetriou*, 1983; *Myers*, 1987]. In terms of (2) this means that the first term in parentheses is much greater than 1, so that (2) can be simplified to a two-parameter power law, as assumed by *Fread and Lewis* [1986]. From this it follows that (4) is also simplified to a two-parameter power law. With these

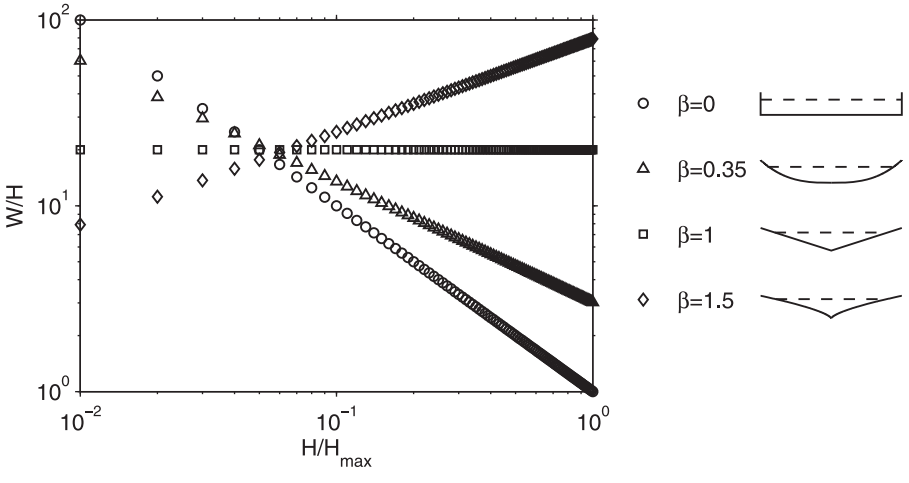

Figure 1. Representation of the power law cross section for different cross-section geometries: rectangular ($\beta = 0$), parabolic ($\beta = 0.35$), triangular ($\beta = 1$), and V shaped ($\beta = 1.5$). For $\beta < 1$ and $\beta > 1$ the cross sections are classified as depth dominant and width dominant, respectively. The vertical axis is the width-depth ratio W/H. On the basis of the channel cross-section power laws (1) and (3) the ratio is equal to $\alpha(\beta+1)h^{\beta-1}$. The horizontal axis is the hydraulic depth H normalized by the maximum hydraulic depth H_{max}.

assumptions, we extend the application of the at-a-site relationships (5)–(7) to the floodplain geometry by replacing α and β in the expressions in Appendix A by their floodplain counterparts.

[13] Indeed, similar expressions to (5)–(7) were empirically derived by *Bhowmik* [1984] for floodplain downstream hydraulic geometry. Here, following a similar approach as previously done for the channel, we use the empirical floodplain scaling relationships proposed by *Dodov and Foufoula-Georgiou* [2005] to account for the effects of scale in floodplain hydraulic geometry. With these relationships we obtain a scale-dependent expression for α_f (see Appendix B2).

[14] We let β and β_f be spatially invariant within a basin, which can be a reasonable assumption many times [*Orlandini and Rosso*, 1998; *Koren et al.*, 2004; *Camporese et al.*, 2010]. Hence, we only consider scale dependency in the hydraulic geometry coefficients. This makes our approach comparable to simple scaling [*Dodov and Foufoula-Georgiou*, 2004].

3. Network Instantaneous Response Function

[15] We describe the IRF model briefly, mainly to emphasize places where our approach differs from previous ones [*Robinson et al.*, 1995; *Paik and Kumar*, 2004], but some repetition is unavoidable. More details about the IRF can be found elsewhere [see, e.g., *Robinson et al.*, 1995; *Saco and Kumar*, 2002a; *Paik and Kumar*, 2004]. For the IRF $f(t)$ we use the inverse Gaussian distribution [*Mesa and Mifflin*, 1986; *Rinaldo et al.*, 1991; *Robinson et al.*, 1995; *Saco and Kumar*, 2002a; *Paik and Kumar*, 2004]:

$$f(t) = \frac{E[L_\gamma]}{\sqrt{4\pi D_n t^3}} \exp\left\{\frac{-\left(E[L_\gamma] - u_n t\right)^2}{4 D_n t}\right\}, \tag{8}$$

where $E[L_\gamma][L]$ is the mean path length of all paths γ in the network, u_n [$L\ T^{-1}$] is the network celerity, and D_n [$L^2\ T^{-1}$] is the network dispersion.

[16] We use the scaling relationship $E[L_\gamma] \sim A_d^{\phi_1}$ to obtain an expression for the mean path length [*Robinson et al.*, 1995]. L_γ is the length for a given path γ, and A_d [L^2] is drainage area. For u_n we employ the following relationship:

$$u_n = p' A_d^{q'+m'} i_e^{m'}. \tag{9}$$

The derivation of (9) and the exact definition of p', q', and m' are included in Appendix C1. Here i_e [$L\ T^{-1}$] is effective rainfall. Note that p' depends on the cross-section parameters α and β, q' depends on β, and m' is the at-a-site mean velocity exponent in (7). The nonlinear relationship $u_n \sim i_e^{m'}$, for a given basin size, has been indicated previously [*Robinson et al.*, 1995; *Saco and Kumar*, 2002b; *Paik and Kumar*, 2004]. We suggest here that this nonlinear dependence may be further related to the cross-section geometry through the relationship between m' and β (see Appendix A for details):

$$m' = 2/(5 + 3\beta). \tag{10}$$

[17] For the network dispersion we use the following expression [after *Saco and Kumar* 2002a]:

$$D_n = D_d + D_{k-g}, \tag{11}$$

where D_d [$L^2\ T^{-1}$] and D_{k-g} [$L^2\ T^{-1}$] are the network hydrodynamic and kinematic-geomorphologic dispersions, respectively. For D_d an expression similar in form to (9) is used (see section C2 for details):

$$D_d = r' A_d^{s'+f'+m'} i_e^{f'+m'}, \tag{12}$$

where r' depends on α and β, s' depends on β only, and $f' + m'$ is the sum of the at-a-site exponents for mean velocity and depth, respectively; f' is given by (see Appendix A for details)

$$f' = 3/(5 + 3\beta). \tag{13}$$

Thus, the nonlinear dependence of $D_d \sim i_e^{f'+m'}$ for a given basin size can be influenced by the cross-section geometry. The other term in (11), D_{k-g}, is given by [*Saco and Kumar*, 2002a]

$$D_{k-g} = \frac{u_n \mathrm{Var}(L'_\gamma)}{2E[L_\gamma]}, \tag{14}$$

where $\mathrm{Var}(L'_\gamma)$ is the variance of the stretched path lengths L'_γ. L'_γ results from the spatial variability of celerity [*Rinaldo et al.*, 1995; *Saco and Kumar*, 2002a]. We use $\mathrm{var}(L'_\gamma) \sim A_d^{\phi_2}$ by treating $\mathrm{Var}(L'_\gamma)$ as independent of i_e. This follows from the averaging used to estimate the network celerity in section C1.

[18] To determine D_k, we subtract D_g from D_{k-g} [*Saco and Kumar*, 2002a]. We define D_g [$L^2\ T^{-1}$] on the basis of the work by *Snell and Sivapalan* [1994],

$$D_g = \frac{u_n \mathrm{Var}(L_\gamma)}{2E[L_\gamma]}, \tag{15}$$

and estimate the variance of the path lengths as $\mathrm{Var}(L_\gamma) \sim A_d^{\phi_4}$ [*Robinson et al.*, 1995]. We use the separation of D_n into D_g, D_k, and D_d to detect and quantify the relative role of cross-section geometry on different flow-routing factors. D_g is used to quantify the influence of the stream network structure [*Rinaldo et al.*, 1991], while D_k and D_d are used to assess the relative importance of the spatial heterogeneity of the local celerity and channel characteristics, respectively.

[19] We obtain an approximate expression for the contribution of the different dispersion mechanisms relative to D_n by combining equations (9)–(15). For this we define the dimensionless quantity η as the ratio of D_d to D_{k-g}. After some manipulations, we arrive at

$$\eta = \frac{D_d}{D_{k-g}} \sim A_d^{s'+f'-q'-\phi_2+\phi_1} i_e^{f'}. \tag{16}$$

Using η, the fraction of the different contributions to D_n is given by

$$\frac{D_d}{D_n}+\frac{D_k}{D_n}+\frac{D_g}{D_n}=\frac{\eta}{(1+\eta)}+\frac{(1-\eta')}{(1+\eta)}+\frac{\eta'}{(1+\eta)}=1, \quad (17)$$

where the ratio of D_g to D_{k-g}, η', is then given by

$$\eta' \sim A_d^{\phi_4-\phi_2}. \quad (18)$$

In terms of η and other previously defined variables, we estimate the variance of the network travel time $\mathrm{Var}(T_n)$ [T^2] [after *Rinaldo et al.*, 1991] as follows:

$$\mathrm{Var}(T_n) \sim A_d^{\phi_2-2(q'+m')} i_e^{-2m'}(1+\eta). \quad (19)$$

The cross-section geometry enters into (19) through the exponents q' and m' and the network dispersion, $1+\eta$. We use $\mathrm{Var}(T_n)$ to quantify the effects of cross-section geometry on the spread, or "attenuation," of the response.

[20] To explore the role of cross-section geometry using the IRF, we will let the power law cross-section coefficient α or α_f be determined by equations (B7) or (B11), respectively, depending on whether flow conditions are in the channel or floodplain. Thus, the effects of α and α_f on the network response enter into the analysis through changes in basin size. On the other hand, the effects of the cross-section exponent β or β_f will be considered by heuristically varying its value within a reasonable range. We will use the dependence of the IRF hydrodynamic parameters on drainage area and effective rainfall to investigate the effects of cross-section geometry across scales and on flow conditions, respectively. To assess more broadly the implications of the proposed framework, we will look at how changes in the slope-area exponent ω affect the IRF hydrodynamic parameters.

4. Case Study

[21] The application of the IRF with parameterized cross sections is demonstrated using the Illinois River basin, with the main outlet chosen at Tahlequah (U.S. Geological Survey (USGS) gauge 07196500). The basin is located at the Oklahoma-Arkansas border and has a drainage area of approximately 2484 km^2. The mean annual rainfall and runoff coefficient for the basin are approximately 1165 mm and 0.30, respectively. A complete description of the basin location and characteristics is given by *Smith et al.* [2004] and *Reed et al.* [2007]. The basin is within the same hydroclimatic region used in a previous floodplain scaling study [*Dodov and Foufoula-Georgiou*, 2005]. The stream network for the Illinois River basin at approximately 100 m resolution was obtained from available DEM data [*Smith et al.*, 2004]. This basin is also selected to allow past modeling results to bear on our discussion [*Koren et al.*, 2004; *Smith et al.*, 2004].

[22] To assess the proposed hydraulic geometry, we compared the analytical expressions in Appendix A against data in the Illinois River, including the outlet gauge and the following four interior gauges (in parentheses are the gauge number and drainage area): Kansas (07196000, $A_d = 285$ km^2), Siloam Springs (07195430, $A_d = 1489$ km^2), Springtown (07195800, $A_d = 36.8$ km^2), and Watts (07195500, $A_d = 1645$ km^2). The location and basin characteristics associated with these gauges are given by *Reed et al.* [2007]. Figure 2a shows an example of the proposed channel and floodplain relationships for the outlet gauge. Figure 2b plots the estimated h ($h_{\mathrm{analytical}}$) from (A2) against the observed values (h_{rating}) for each of the five gauges. From Figure 2b it is seen that the proposed analytical expressions match the USGS ratings reasonably well. The values tend to be within the $h_{\mathrm{rating}} \pm 0.1\ h_{\mathrm{rating}}$ bound representing the likely error in h_{rating} [*Kennedy*, 1984]. Further, in Figure 3 we compare the estimated velocity against observed values for the gauges with velocity data. Overall, Figure 3 shows a reasonable ability to capture the trends in the channel and floodplain values, although the floodplain comparison in Figures 3a and 3b is difficult to perform given the few data that are available. In addition, we note that at Tahlequah (Figure 3d), the largest basin size considered here, the channel velocity appears to be overestimated. This is possibly due to local variability not captured by the average values of hydraulic geometry.

[23] The application of the IRF requires several fluvial geomorphological empirical parameters. The parameters and their value for the Illinois River are summarized in Table 1. Most of the parameters can be estimated from the literature. We estimated the bankfull (ψ_1, ψ_2, ψ_4, θ_1, θ_2, and θ_4), floodplain (ψ_3, θ_3, and ξ), and roughness coefficient (λ and τ) parameters from previous studies [*Dutnell*, 2000; *Koren et al.*, 2004; *Dodov and Foufoula-Georgiou*, 2005], while the parameters in $E[L_\gamma]$ (ς_1 and ϕ_1), $\mathrm{Var}(L'_\gamma)$ (ς_2 and ϕ_2), L_m (ς_3 and ϕ_3), $\mathrm{Var}(L_\gamma)$ (ς_4 and ϕ_4), and the slope-area relationship (Ω and ω) were estimated using the DEM data.

[24] The regression equations used to estimate the scaling relationships for $E[L_\gamma]$, $\mathrm{Var}(L'_\gamma)$, L_m, and $\mathrm{Var}(L_\gamma)$ yielded R^2 values of 0.97, 0.96, 0.94, and 0.96, respectively. The coefficient ς_2 and the exponent ϕ_2 used to determine $\mathrm{Var}(L'_\gamma)$ were found to be only weakly dependent on β and to vary little between channel and floodplain. Thus, to simplify our discussion, the single set of values shown in Table 1 was adopted. The single values selected correspond to the value of β implied by the average of the at-a-site exponent for mean velocity of *Leopold and Maddock* [1953]. The parameters in the slope-area relationship were estimated following the approach of *Tarboton et al.* [1989].

[25] Furthermore, on the basis of the analysis of *Osterkamp et al.* [1983], the influence of the cross-section geometry, through the ratio W/H, on the bankfull exponent θ_1 in $A_{bf} \sim A_d^{\theta_1}$ (equation (B4)) tends to be small. Thus, we let θ_1 be constant. The exponent θ_2 in $Q_{bf} \sim A_d^{\theta_2}$ (equation (B5)) has a complex underlying structure. It has been tied to first order to macroscopic factors such as the stream network and the rainfall characteristics [*Mantilla et al.*, 2006] but not to the cross-section form. Therefore we assume θ_2 to be constant within a basin as well. The exponent τ in $n \sim A_d^{\tau}$ could also be potentially affected by β. However, the estimation of n for the entire stream network can be quite uncertain [*Sturm*, 2001; *Orlandini*, 2002], resulting many times in $n \sim A_d^{\tau}$ having a low predictability [*Orlandini*, 2002]. Taking this into consideration, we foresee that β will be weakly related to τ. Hence, we assume τ to be constant.

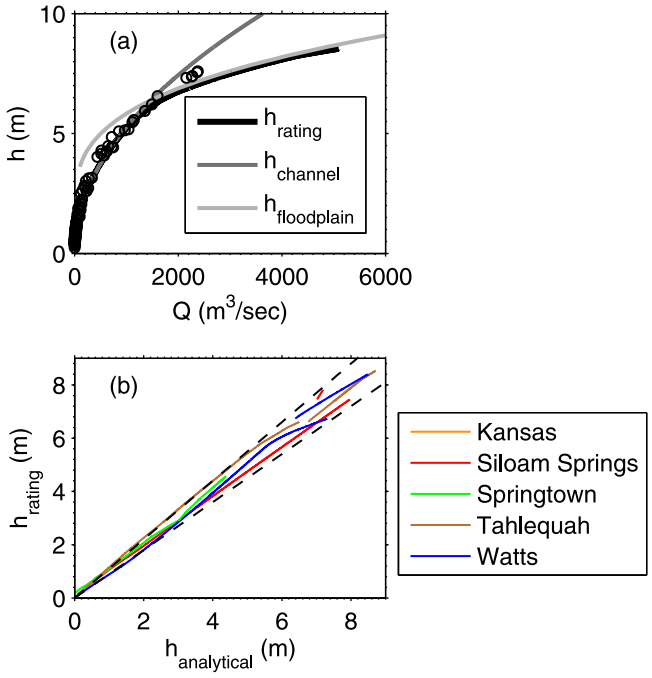

Figure 2. (a) Comparison of the proposed $h \sim Q^{f'}$ relationship for both channel (h_{channel}) and floodplain ($h_{\text{floodplain}}$) against the U.S. Geological Survey rating (h_{rating}) and gauged values (denoted by circles) at Tahlequah. (b) Measured rating (h_{rating}) versus proposed ($h_{\text{analytical}}$) for the outlet and four interior gauges in the Illinois River. The dashed lines represent a 10% error in the ratings ($h_{\text{rating}} \pm 0.1\ h_{\text{rating}}$). In all cases shown, $\beta = 0.35$ for the channel and 1.5 for the floodplain.

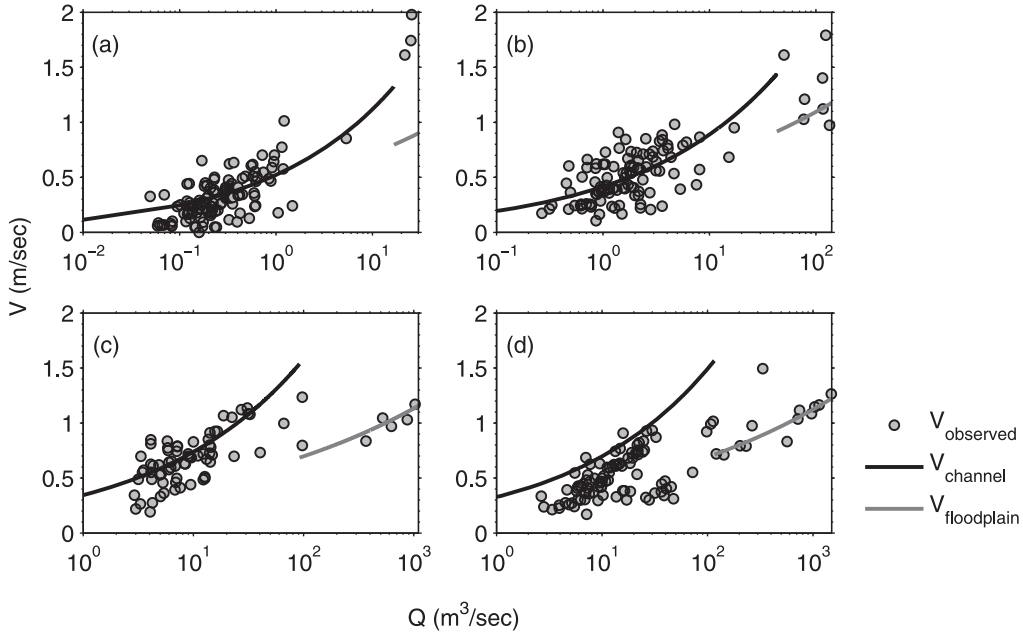

Figure 3. Comparison of the proposed $V \sim Q^{m'}$ relationship for both channel (V_{channel}) and floodplain ($V_{\text{floodplain}}$) against measured values at the following USGS gauges: (a) Springtown ($A_d = 36.8$ km^2), (b) Kansas ($A_d = 285$ km^2), (c) Siloam Springs ($A_d = 1489$ km^2), and (d) Tahlequah ($A_d = 2484$ km^2). Here $\beta = 0.35$ for the channel and 1.5 for the floodplain. The discontinuity between V_{channel} and $V_{\text{floodplain}}$ is set at the bankfull discharge.

Table 1. Summary of the Coefficients and Exponents in the Empirical Geomorphological Relationships Employed

Parameter	Symbol	Value
Expected value of path lengths coefficient	ς_1	0.94
Expected value of path lengths exponent	ϕ_1	0.54
Variance of stretched path lengths coefficient	ς_2	0.12
Variance of stretched path lengths exponent	ϕ_2	1.12
Main stream lengths coefficient	ς_3	1.062
Main stream lengths exponent	ϕ_3	0.6
Variance of path lengths coefficient	ς_4	0.092
Variance of path lengths exponent	ϕ_4	1.13
Bankfull cross-section coefficient[a]	ψ_1	2.78
Bankfull cross-section exponent[a]	θ_1	0.42
Bankfull discharge coefficient[a]	ψ_2	3.19
Bankfull discharge exponent[a]	θ_2	0.46
Bankfull depth coefficient[a]	ψ_4	0.77
Bankfull depth exponent[a]	θ_4	0.089
Floodplain width coefficient	ψ_3	5
Floodplain width exponent[b]	θ_3	0.3
Floodplain depth coefficient[b]	ξ	0.6
Roughness coefficient[c]	λ	0.065
Roughness exponent[c]	τ	−0.084
Slope-area coefficient	Ω	0.015
Slope-area exponent	ω	−0.31

[a]Values obtained from *Dutnell* [2000].
[b]Values estimated from *Dodov and Foufoula-Georgiou* [2005].
[c]Values estimated from *Koren et al.* [2004].

[26] To evaluate the effects of channel cross-section geometry across basin sizes, we assume a spatially uniform effective rainfall of 0.17 mm h^{-1}. This value of i_e results in an instantaneous streamflow that is approximately just at bankfull at the main basin outlet. It was estimated by dividing the bankfull flow by the drainage area at the main basin outlet. For the floodplain we assume a value of $i_e = 4.7$ mm h^{-1}. This value of i_e was approximated by dividing the 100 year peak flow over the drainage area at the main outlet. This results in above-bankfull flow conditions for the entire range of drainage areas that we consider here. The peak flow for a given return period was obtained from *Tortorelli* [1997].

5. Results and Discussion

5.1. Network Hydrodynamic Parameters

[27] The network celerity u_n and hydrodynamic dispersion D_d are shown in Figures 4a and 4b, respectively, as a function of basin size for different channel cross-section geometries, as specified by β. In Figure 4a, the trend for u_n is to increase as β increases across basin sizes. This means that for the expanding V-shaped channel cross section (i.e., the width-dominant cross sections), u_n is faster than for the rectangular and parabolic channel cross sections (i.e., the depth-dominant cross sections). This is the case here because for low flows the V-shaped cross section is narrow relative to the bankfull width. In terms of the power law cross section in (1) this is seen as $W/H \to 0$ as $h \to 0$ for $\beta > 1$, while for $\beta < 1$, $W/H \to \infty$ as $h \to 0$. This trend also produces a larger coefficient p' in (9) as β increases. Consistently, the trend in the channel for D_d is similar to the trend experienced by u_n. D_d tends to be larger for the

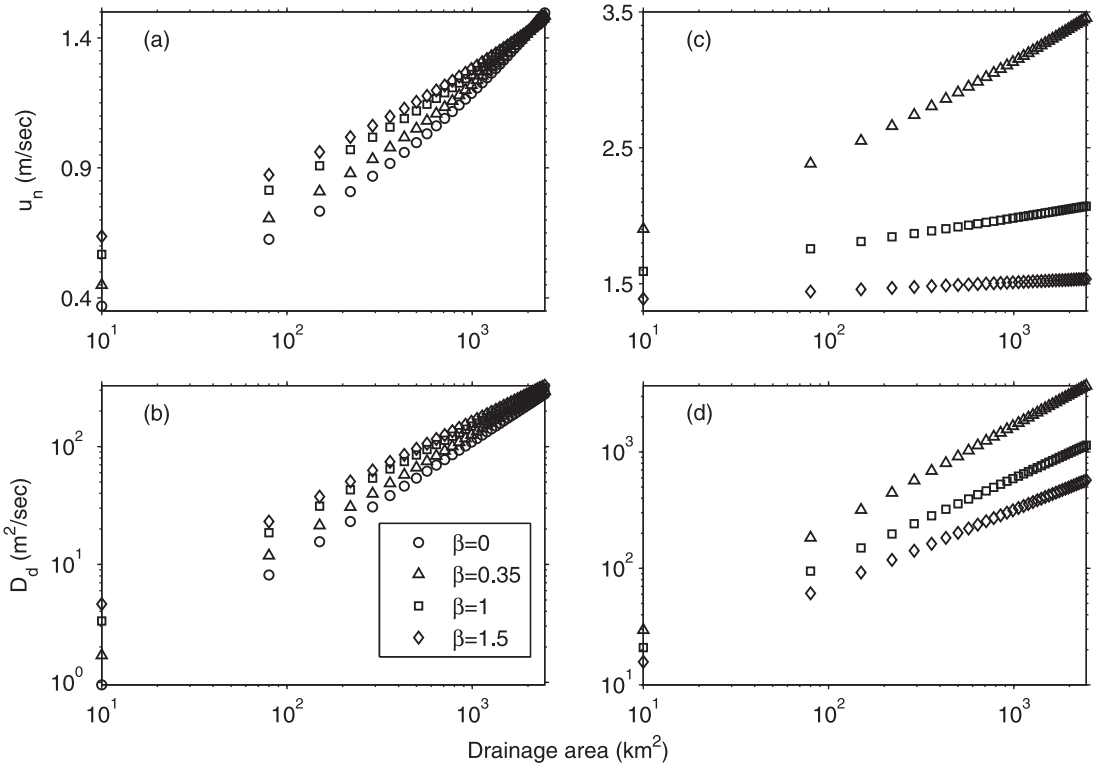

Figure 4. Network (a) celerity u_n and (b) hydrodynamic dispersion D_d for the channel ($i_e = 0.17$ mm h^{-1}) as a function of drainage area. Network (c) celerity and (d) hydrodynamic dispersion for the floodplain ($i_e = 4.7$ mm h^{-1}). Here β represents different cross-section geometries: rectangular ($\beta = 0$), parabolic ($\beta = 0.35$), triangular ($\beta = 1$), and V shaped ($\beta = 1.5$).

width-dominant channel cross sections, as illustrated in Figure 4b.

[28] The effect of channel geometry on the hydrodynamic parameters is also influenced by the bankfull scaling relationships, equations (B4) and (B5). These are used to quantify the spatial variability of the channel cross-section coefficient α (see section B1). Specifically, (B4) and (B5) delimit the spatial extent of channel flow conditions. They also, on the basis of continuity, have the effect of fixing the channel velocity field at bankfull. This contributes in this case to the convergence at the main outlet of the channel u_n and D_d in Figures 4a and 4b (top right corner), respectively, for the different values of β.

[29] For the floodplain geometry, the width-dominant cross section tends to produce a lower u_n (see Figure 4c) and D_d (see Figure 4d) across basin sizes. Thus, in terms of β, for the floodplain cross section the trend for u_n and D_d reverses when compared to the channel cross section. For example, if the channel and floodplain are both characterized by a depth-dominant cross section, then the channel cross section will tend to decrease the network celerity relative to the same flow condition in a width-dominant cross section, while for a given high-flow condition the depth-dominant floodplain cross section will tend to increase the network celerity relative to the width-dominant cross section. Conceivably, this could have a controlling effect on the range of variability of the network hydrodynamic parameters. In this case, the range would be greatest when both the channel and floodplain are characterized by depth-dominant cross sections. The floodplain scaling relationships (B8) and (B9) influence how fast the floodplain cross section grows with basin size [*Bhowmik*, 1984; *Dodov and Foufoula-Georgiou*, 2005; *Nardi et al.*, 2006]. They help specify in this case the size of the floodplain along the stream network through the coefficient α_f.

[30] Alternatively, from Figure 4, we interpret the dynamic influence of cross-section geometry on the hydrodynamic parameters in terms of storage or, in contradistinction, conveyance. The depth-dominant channel cross section may be seen as acting as storage for the very low flows, relative to the larger celerity of the width-dominant channel cross section. As the flow approaches bankfull the channel geometry acts as conveyance. This is because the network celerity in the depth-dominant cross sections (i.e., the cross sections with the lower celerity) tends to increase at a faster rate with increasing flow. This results, as illustrated in Figure 4a, in the network celerity being approximately the same for the different cross-section forms near the main basin outlet. On the other hand, when the flow is high and the floodplain geometry is dominant, the cross-section geometry can play two different roles. The floodplain with depth-dominant cross section increases the network celerity, acting more as conveyance, while the floodplain characterized by width-dominant cross sections slows the network celerity, prolonging the storage effect.

[31] Using the slope-area exponent ω and the exponents q' and s' in u_n and D_d, respectively, we assess more broadly the implications of the proposed parameterization. For the channel, q' does not depend explicitly on ω. However, through θ_1 the slope-area exponent ω can potentially affect the channel q'. The interrelationship between θ_1 and ω was indicated, quite generally, by *Molnár and Ramírez* [1998]. What matters here is that the previous means that the channel q' can vary between basins depending on the basin-wide values of ω, θ_1, and θ_2. For example, when θ_2 is larger than the value used here, the channel u_n will be greater for a given basin size. The effect of ω on the channel is more evident in the coefficient for the at-a-site expression $V \sim Q^{m'}$ (equation (A4)). In (A4) it is straightforward to recognize that for a given basin size, as ω decreases, or s_o is smaller, the velocity slows down. Thus, as the terrain becomes flat, V and hence u_n tend to decrease. The opposite behavior is expected for u_n when the terrain is steeper. The effect of ω on the floodplain u_n is similar; as ω decreases, q' tends to decrease as well, resulting in lower floodplain u_n values.

[32] The effect of ω on D_d through the exponent s' is the same for the channel and floodplain; D_d tends to increase as ω decreases. Thus, in basins where ω is less than in the Illinois River basin, we expect a lower u_n and a higher D_d value. Nonetheless, the net effect of changes in q' and s' on u_n and D_d, respectively, will depend on the interplay between ω and the other exponents affecting our estimate of q' and s'. However, once these other exponents are defined for a given basin, relative to these values, the trends shown in Figure 4 will be similar.

[33] Viewed as an order of magnitude estimate, our analysis of the network hydrodynamic parameters illustrated in Figure 4 indicates that the channel and floodplain cross-section geometry have an effect on the dynamics of the network response. We will analyze this effect further in sections 5.2–5.4.

5.2. Network Dispersion and Variance of *f*(*t*)

[34] Figure 5a shows the fraction of the contribution of the three dispersion mechanisms (i.e., geomorphic (D_g), kinematic (D_k), and hydrodynamic (D_d)) as a function of drainage area for two channel cross-section geometries (i.e., $\beta = 0.35$ and $\beta = 1.5$). The different dispersion mechanisms are estimated using equation (17). In Figure 5a, D_g has a dominant influence over both D_d and D_k, as indicated previously [*Rinaldo et al.*, 1991; *Saco and Kumar*, 2002a, 2002b]. Further, D_g is affected little by the channel cross-section geometry, while D_d and D_k show a more noticeable effect. The trend is for D_d to increase and D_k to decrease as the basin size increases or as flow conditions approach bankfull. In terms of β, the main effect is for the width-dominant cross section to have a greater D_d and a smaller D_k across basin sizes. On the basis of our interpretation of D_d and D_k, this indicates that the spatial variability of channel characteristics becomes more important for the width-dominant cross sections.

[35] For the floodplain, a similar comparison of the dispersion mechanisms is shown in Figure 5b. In Figure 5b it is seen that D_g continues to have a dominant effect over both D_d and D_k across basin sizes. However, two main differences with respect to the channel cross section are apparent. First, D_d continues to increase across basin sizes, but now the depth-dominant cross section results in a larger D_d. Second, for the very high floodplain flows, D_d can become greater than D_k. This suggests that only in situations of extreme flood and relatively large drainage area can the spatial variability of the floodplain geometry become more dominant than that of the celerity. Thus, in terms of D_n, the

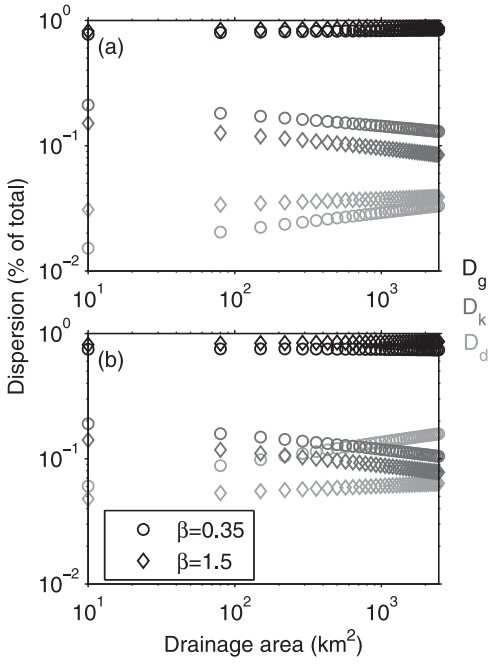

Figure 5. Contribution of the different network dispersion mechanisms (geomorphic (D_g), kinematic (D_k), and hydrodynamic (D_d)) for the (a) channel ($i_e = 0.17$ mm h^{-1}) and (b) floodplain ($i_e = 4.7$ mm h^{-1}) as a function of drainage area. D_g is shown in black, D_k is in dark gray, and D_d is in light gray. Here $\beta = 0.35$ (circles) and $\beta = 1.5$ (diamonds) are for rectangular and V-shaped cross-section forms, respectively.

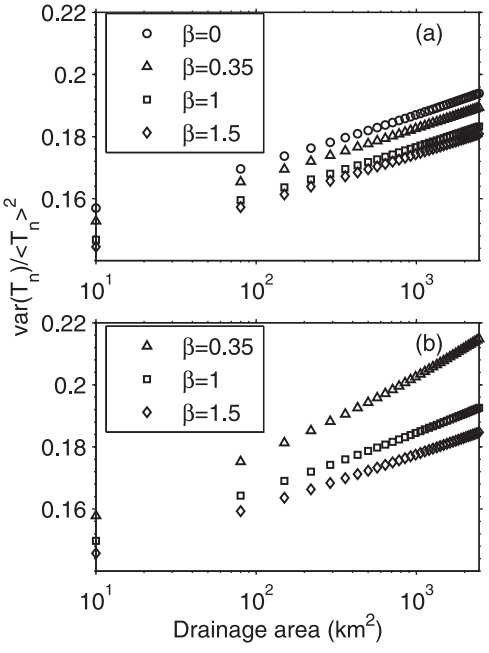

Figure 6. Normalized variance of the network travel time $\mathrm{Var}(T_n)/\langle T_n\rangle^2$ for the (a) channel ($i_e = 0.17$ mm h^{-1}) and (b) floodplain ($i_e = 4.7$ mm h^{-1}) as a function of drainage area.

channel and floodplain cross-section geometry influence the relative contribution of D_d and D_k. The differences between the channel and floodplain geometry are mainly reflected in D_d.

[36] To examine the combined effects of the network celerity and dispersion on travel times, we plot in Figures 6a and 6b the normalized variance of the network travel time $\mathrm{Var}(T_n)/\langle T_n\rangle^2$ for the channel and floodplain, respectively. The variance is estimated using equation (19), and the normalizing quantity is estimated as the square of $E[L_\gamma]$ over u_n. The normalized variance can be seen as quantifying the relative attenuation of the response. In fact, it is equivalent to the ratio of the network dispersion over the advection or, namely, the inverse of the network Péclet number. Therefore, a large $\mathrm{Var}(T_n)/\langle T_n\rangle^2$ indicates a low Péclet number and a more dispersed response, and a low $\mathrm{Var}(T_n)/\langle T_n\rangle^2$ corresponds to a high Péclet number and a more peaked response. Figures 6a and 6b show that the normalized variance is greater for the depth-dominant cross sections in both the channel and floodplain, respectively (i.e., $\mathrm{Var}(T_n)/\langle T_n\rangle^2$ increases as β decreases across basin sizes). Additionally, both the channel and floodplain have a comparable dispersive influence on the response in terms of the magnitude of $\mathrm{Var}(T_n)/\langle T_n\rangle^2$. Thus, the channel and floodplain geometry take on similar roles in terms of $\mathrm{Var}(T_n)/\langle T_n\rangle^2$. The only difference between the channel and floodplain in Figure 6 is that the normalized variance shows a somewhat stronger sensitivity to the floodplain geometry. The range of $\mathrm{Var}(T_n)/\langle T_n\rangle^2$ tends to be greater for the floodplain at a given basin size, and it tends to widen as the basin size increases. This means that the floodplain geometry has a relatively greater ability to influence the response's attenuation.

[37] More broadly, in basins where the slope-area exponent is less than in the Illinois River basin, the trends shown in Figures 5 and 6 will be similar. However, D_d will tend to play a larger role relative to the other dispersion mechanisms (i.e., D_g and D_k) since a lower ω increases the value of D_d. In terms of Figure 5, this means that D_d will take a larger percent of the total contribution across basin sizes. For $\mathrm{Var}(T_n)/\langle T_n\rangle^2$ in Figure 6 this means that the response will be less peaked across basin sizes as ω decreases for a given flow condition. Thus, as one might expect, in basins with flat terrain where ω is small the response tends to be more attenuated relative to the same flow condition in a steep terrain where ω is larger.

[38] Despite the normalized variance being similar in Figures 6a and 6b, ultimately, the effects of the channel and floodplain geometry on the IRF are different owing to the different flow frequencies associated with them. This is illustrated in Figure 7 using a hypothetical channel scenario. In Figure 7 we allow the channel cross section to hypothetically convey the floodplain flow. With this we want to emphasize three main points. First, relative to the channel geometry, the floodplain increases the variance of the network travel time and attenuates the response. Second, as a corollary, neglecting the effects of floodplain geometry can have a pronounced effect on the network response for the high flows. For example, contrasting in Figure 7 the IRFs for the Illinois River (i.e., $\beta = 0.35$ and $\beta_f = 1.5$), the peak of the IRF is approximately twice as large if the channel hydraulic geometry is employed instead of the floodplain (the peak is 0.15 h^{-1} for the channel and

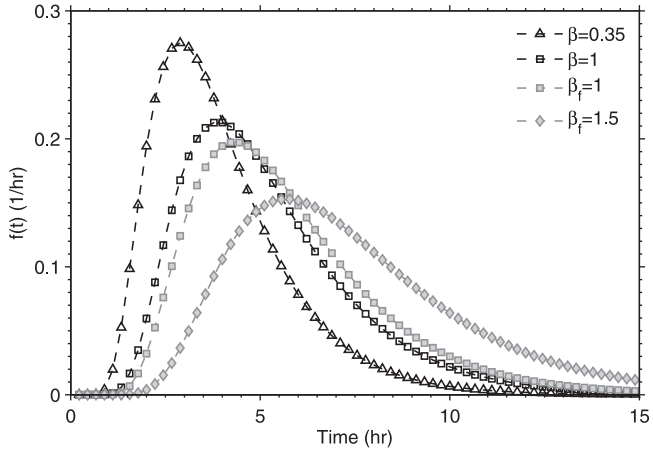

Figure 7. Effect of floodplain cross-section geometry on the IRF with $i_e = 4.7$ mm h^{-1} (gray dashed lines). In a hypothetical scenario, the IRFs for the channel cross sections shown are estimated using the same i_e value as in the floodplain (black dashed lines).

0.28 h^{-1} for the floodplain). Third, the channel geometry tends to approach the floodplain response as β increases. In our case, the IRF for the channel with $\beta = 1$ and the IRF for the floodplain with the same β are nearly coincident in Figure 7. This suggests further that the width-dominant cross section may be generally effective for capturing high-flow dynamics under the single power law channel cross section. Conceivably, the latter may be a useful compensating mechanism in modeling situations where the channel and floodplain are not explicitly distinguished. Our experience with estimating parameters for the single power law approach used in HL-RDHM is consistent with this observation. When we estimate shapes using USGS flow measurements and emphasizing high flows, we find $\beta > 1$ in most cases.

5.3. Network Response Nonlinearity

[39] We follow the approach of *Paik and Kumar* [2004] to determine the time to peak t_p and peak flow $f(t = t_p)$, or simply $f(t_p)$, of the IRF. The complete expressions for t_p and $f(t_p)$ are omitted since they can be found elsewhere [see *Paik and Kumar*, 2004]. What matters for our purposes is that using (8), t_p and $f(t_p)$ can be written for a given basin size as follows:

$$t_p \sim i_e^{-m'}, \tag{20}$$

$$f(t_p) \sim i_e^{m'}. \tag{21}$$

Through the at-a-site mean velocity exponent m', expressions (20) and (21) are directly linked to the cross-section geometry. Using the floodplain hydraulic geometry [*Bhowmik*, 1984; *Nardi et al.*, 2006], (20) and (21) can be extended to the floodplain. The value of the coefficients in (20) and (21) will differ between the channel and floodplain geometry because of the different scaling relationships employed in estimating α and α_f.

[40] Figure 8a illustrates the behavior of (20) for the channel at the main basin outlet. From Figure 8a, t_p is smaller for the width-dominant cross sections for increasing effective rainfall, as expected from the effect of cross-section geometry on the IRF parameters reported earlier. Consistent with the effects of β on t_p, $f(t_p)$ is larger for the width-dominant cross sections, as illustrated in Figure 8b. Thus, the width-dominant cross section results in a more peaked channel response. It is straightforward to imply that for the floodplain, on the basis of our previous results, the opposite is the case here (i.e., the response has a shorter t_p and larger $f(t_p)$ when $\beta < 1$). The floodplain response is then more peaked for the depth-dominant cross section.

[41] Figure 8 also indicates that the rate of change of t_p and $f(t_p)$ with i_e decreases when β increases for both the channel and floodplain. This means that the response nonlinearity, as manifested in the dependence of t_p and $f(t_p)$ on i_e [*Wang et al.*, 1981; *Paik and Kumar*, 2004], tends to decrease as β increases since this reduces the value of the exponent m'. For example, if we let the channel have a value of $\beta = 0.35$ (the value implied by the average exponents of *Leopold and Maddock* [1953]) and the floodplain have a value of $\beta > 1$, one expects a more linear response for the floodplain than the channel. The latter rests on the condition, based on continuity and the effect of β on the hydraulic geometry exponents, that b' increases and f' decreases for the floodplain. Indeed, the condition of a lower f' for the floodplain is often manifested in rating curves (i.e., the at-a-site relationship between stage and discharge), requiring the application of a separate stage-discharge floodplain power law [*Kennedy*, 1984]. In our case at hand, what matters is that a lower f' implies a larger β and consequently a larger b' for the floodplain. This suggests that the floodplain geometry can interact with the flow to reduce the nonlinear dependency described by (20) and (21). The controlling mechanism for this seems to be the increase in b' since b' is more sensitive to increases in β than f'. Taking, as a measure of relative sensitivity, the ratio of the absolute value of the derivative of b' and f' with respect to β (i.e., $|db'/d\beta|/|df'/d\beta|$) results in a value of 5/3, indicating b' is more sensitive to changes in β.

5.4. Basin Dispersion

[42] We use the basin dispersion D_b in this section to examine the effect of cross-section geometry on the relative influence of hillslopes and the stream network. For D_b we employ the following expression [*Robinson et al.*, 1995; *Botter and Rinaldo*, 2003; *D'Odorico and Rigon*, 2003]:

$$D_b = D_{bn} + D_{bh} = u_b^3 \frac{[\mathrm{Var}(T_n) + \mathrm{Var}(T_h)]}{2(E[L_\gamma] + E[L_h])}. \tag{22}$$

D_{bn} and D_{bh} partition D_b into a stream network and a hillslope contribution, respectively, on the basis of $\mathrm{Var}(T_n)$ and the hillslope variance $\mathrm{Var}(T_h)$. Here u_b is estimated as the weighted sum of u_n and the hillslope velocity [*Robinson et al.*, 1995]. The weighting is done using $E[L_\gamma]$ and the mean hillslope length $E[L_h]$. Through u_b it is possible for the stream cross-section geometry to influence D_{bh}. Hence, D_{bh} represents the relative influence of hillslopes on the aggregated basin-wide dispersion, i.e., the effect of hillslopes at the basin outlet. Further, equation (22) assumes that the hillslope and network paths are independent [*van der Tak and Bras*, 1990; *Robinson et al.*, 1995; *Botter and Rinaldo*, 2003; *D'Odorico and Rigon*, 2003].

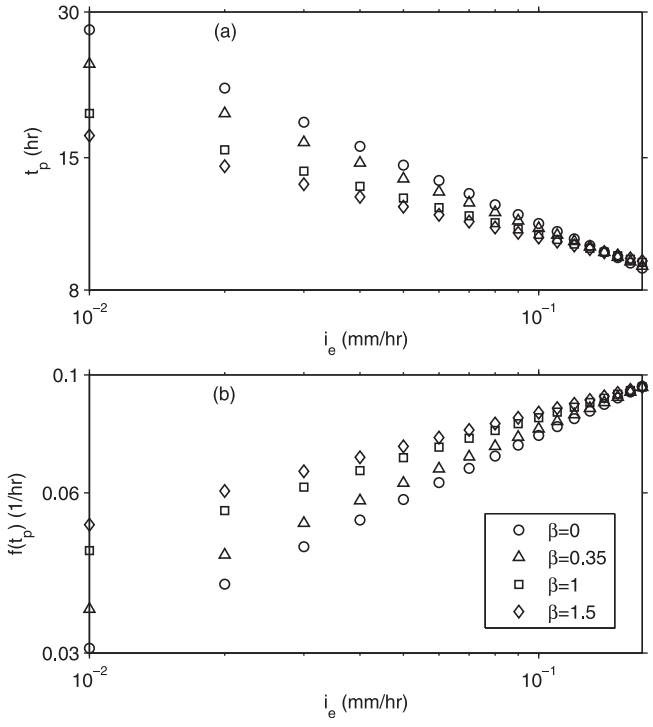

Figure 8. IRF time to peak t_p and peak flow $f(t_p)$ as a function of effective rainfall i_e at the main basin outlet for the channel cross-section geometry. The lower bound for i_e is selected to be arbitrarily very small. The upper bound is determined by dividing the bankfull flow over the drainage area at the main basin outlet.

[43] In equation (22), $E[L_h]$ is determined from the average value of drainage density [*van der Tak and Bras*, 1990; *Rodriguez-Iturbe and Rinaldo*, 1997], which was estimated to be 2.5 km^{-1} for the hydroclimatic region of this study by *Koren et al.* [2004]. The hillslope velocity is assumed to be characterized by a quenched exponential distribution [*Botter and Rinaldo*, 2003], with a mean value of 0.008 m s^{-1} and a minimum threshold of 0.002 m s^{-1}. This velocity scale corresponds approximately to the one implied by the parameter used to model fast subsurface runoff in a previous study of the Illinois River using HL-RDHM [*Koren et al.*, 2004]. We use the hillslope subsurface velocity model for both low- and high-flow conditions. $\mathrm{Var}(T_h)$ is estimated from the hillslope velocity model and $E[L_h]$.

[44] Figure 9 shows the dispersion separated into network and hillslope contributions as a function of drainage area for the channel (Figure 9a) and floodplain (Figure 9b). In Figures 9a and 9b, the cross-section geometry is shown to influence the quantification and partitioning of the basin dispersion into hillslope and network contributions. This influence is more pronounced for the floodplain, where the cross-section geometry can affect the extent of the control of hillslope dispersion across basin sizes. For example, in Figure 9b, the stream network becomes equally dominant (i.e., contributes the same as the hillslope dispersion to the total dispersion) at approximately the main basin outlet for the V-shaped cross section ($\beta = 1.5$), whereas for the parabolic cross section ($\beta = 0.35$) the hillslopes contribute more to D_b across basin sizes. In physical terms, the widening of the floodplain cross section, expressed through the power law cross section with increasing β and the scaling relationships (B8) and (B9), when compared to the channel cross section, tends to slow the response (i.e., decrease the network celerity) and increase the attenuation (i.e., increase the variance of the network travel time). Both of these effects in this case can decrease the spatial extent of the relative influence of hillslopes on the basin dispersion for the high floodplain flows.

6. Summary and Conclusions

[45] The IRF was used to examine the role of cross-section geometry on the basin response because it provides a unified framework for assessing the influence of different flow-routing factors, the effects of the spatial variability of hydrodynamic parameters, and the response nonlinearity. The cross-section geometry was included in the IRF by assuming a power law cross section that was, in turn, used to obtain analytical expressions for the at-a-site hydraulic geometry. To account for the spatial variability of the at-a-site hydraulic geometry, the coefficients in these expressions were related to the drainage area. These coefficients were also used to differentiate between channel and floodplain cross sections, with the support of fluvial geomorphological scaling relationships and simplifying assumptions about the channel-floodplain interaction.

[46] On the basis of the analysis performed using data for the Illinois River basin, we found for the channel that the depth-dominant cross sections tend to produce a lower network celerity and hydrodynamic dispersion than width-dominant cross sections, whereas in the floodplain we found that this trend reverses, particularly for the higher flows. For the network dispersion, geomorphic dispersion

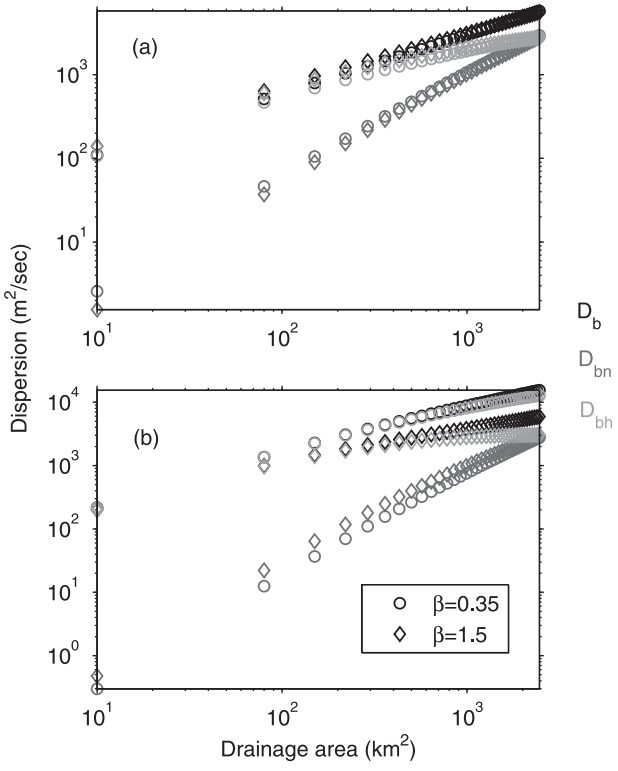

Figure 9. Effect of cross-section geometry on the basin dispersion D_b for the (a) channel ($i_e = 0.17$ mm h^{-1}) and (b) floodplain ($i_e = 4.7$ mm h^{-1}) across basin sizes. D_b is separated into network (D_{bn}) and hillslope (D_{bh}) dispersion on the basis of the network and hillslope variance. D_b is shown in black, D_{bn} is in dark gray, and D_{bh} is in light gray.

was found to be dominant and affected little by the cross-section geometry. However, in terms of the relative kinematic and hydrodynamic contributions to the network dispersion, the cross-section geometry can have a noticeable effect. The width-dominant cross sections tend to decrease the kinematic contribution for both the channel and floodplain, while the depth-dominant cross sections tend to decrease the hydrodynamic contribution for the channel and vice versa for the floodplain. In addition, because the kinematic dispersion tends to decrease across basin sizes while the hydrodynamic increases, we suggest that the spatial variability of channel characteristics is more important for width-dominant cross sections in the channel and depth-dominant in the floodplain. This may help to identify those situations where cross section data for the stream network is most important.

[47] In terms of the normalized variance of the network travel time, we found the channel and floodplain cross-section geometries play a similar role. Both have a comparable network dispersive effect relative to advection. Also, the depth-dominant cross sections produce the greatest normalized variance in both. However, the normalized variance shows a somewhat stronger sensitivity to the floodplain geometry. The nonlinear dependence of the response was found to decrease for the width-dominant cross sections by reducing the value of the at-a-site mean velocity exponent. Further, we suggest that the at-a-site rate of increase of the floodplain width with discharge may act as a linearizing mechanism at high flows.

[48] For the basin response the magnitude and partition of the basin dispersion into hillslope and network components may be influenced by the cross-section geometry. We found this to be more relevant for the floodplain, where depending on the cross-section geometry, the scale at which the hillslope dispersive effect becomes less dominant than the network dispersive effect may vary. The trend is for the width-dominant cross section to reduce the influence of the hillslope dispersive effect the most.

[49] Overall, we find manifested through the IRF notable differences between the channel and floodplain cross sections. We also find that the specific form of the channel or floodplain cross section can have an important influence on the response.

Appendix A: Analytical Representation of the At-a-Site Hydraulic Geometry

[50] To derive the at-a-site hydraulic geometry, we assume that the hydraulic radius in the Manning equation can be approximated by the hydraulic depth H, which is defined as A/W. This assumption may be reasonable for rivers [*Leopold and Maddock*, 1953; *Wang et al.*, 1981; *Fread and Lewis*, 1986; *Orlandini*, 2002; *Dingman*, 2007], but we recognize that it becomes more useful as the basin size increases. With this we write the combined Manning and continuity equation as follows:

$$Q = \frac{s_o^{1/2}}{n}\left(\frac{A^{5/2}}{W}\right)^{2/3}, \tag{A1}$$

where s_o is local channel bed slope and n is the roughness coefficient. Substituting (1) and (3) into (A1), simplifying, and inverting the expression to find $h \sim Q^{f'}$, we arrive at

$$h = \left[\frac{n(\beta+1)^{5/3}}{s_o^{1/2}\alpha}\right]^{\frac{3}{5+3\beta}} Q^{\frac{3}{5+3\beta}}, \tag{A2}$$

where $f' = 3/(5+3\beta)$. Equation (A2) is divided through by $(\beta+1)$ to obtain an expression for $H \sim Q^{f'}$. Also, by substituting (A2) into (1) and simplifying, the following expression can be obtained for $W \sim Q^{b'}$:

$$W = \alpha^{\frac{5}{5+3\beta}}\left[\frac{n(\beta+1)^{5/3}}{s_o^{1/2}}\right]^{\frac{3\beta}{5+3\beta}} Q^{\frac{3\beta}{5+3\beta}}, \tag{A3}$$

where $b' = 3\beta/(5+3\beta)$. Similarly, noting that A/W is equal to $h/(\beta+1)$, substituting (A2) into (A1), after dividing through by A, yields an expression for $V \sim Q^{m'}$:

$$V = \left\{\frac{1}{\left[(\beta+1)^{\beta}\alpha\right]^2}\left(\frac{s_o^{3/2}}{n^3}\right)^{1+\beta}\right\}^{\frac{1}{5+3\beta}} Q^{\frac{2}{5+3\beta}}, \tag{A4}$$

where $m' = 2/(5+3\beta)$. Equations (A2), (A3), and (A4) are written in compact form in section 2.2 so that they

appear just as the at-a-site expressions of *Leopold and Maddock* [1953].

Appendix B: Scale Effects on the Coefficient of the Power Law Cross Section

B1. Channel Cross-Section Coefficient α

[51] To find an expression for α, H (i.e., $h/(\beta+1)$) is multiplied by W in (A3) to obtain $A \sim Q^{f'+b'}$, where h is given by (A2) and A [L^2] is the cross-sectional area. Then α is isolated from the expression $A \sim Q^{f'+b'}$ on the basis of reference values (bankfull conditions) for A and Q [*Orlandini and Rosso*, 1998] as follows:

$$\alpha = \frac{1}{(\beta+1)^{\beta}} \left(\frac{A_{\mathrm{bf}}^{\frac{\beta+5/3}{\beta+1}} s_o^{1/2}}{Q_{\mathrm{bf}} n} \right)^{\frac{3(\beta+1)}{2}}. \tag{B1}$$

For the local slope and roughness coefficient the following empirical relationships are used:

$$s_o = \Omega A_d^{\omega}, \tag{B2}$$

$$n = \lambda A_d^{\tau}. \tag{B3}$$

A_d [L^2] is drainage area. Equation (B2) is the well-known slope-area relationship [see, e.g., *Tarboton et al.*, 1989; *Rodriguez-Iturbe and Rinaldo*, 1997]. Equation (B3) has been suggested by various researchers [*Leopold and Maddock*, 1953; *Osterkamp et al.*, 1983; *Orlandini*, 2002], and we use the expression reported by *Koren et al.* [2004]. The bankfull relationships for A_{bf} and Q_{bf} are

$$A_{\mathrm{bf}} = \psi_1 A_d^{\theta_1}, \tag{B4}$$

$$Q_{\mathrm{bf}} = \psi_2 A_d^{\theta_2}. \tag{B5}$$

Inserting (B2), (B3), (B4), and (B5) into (B1) yields the following expression for $\alpha \sim A_d^{\beta'}$:

$$\alpha = (\beta+1)^{-\beta} \left(\frac{\Omega^{1/2} \psi_1^{(1-m')^{-1}}}{\lambda \psi_2} \right)^{\frac{3}{2}(1+\beta)} \left(A_d^{\frac{3(\beta+1)}{2}} \right)^{\frac{1}{2}\omega - \tau + \theta_1 (1-m')^{-1} - \theta_2}, \tag{B6}$$

which we write in compact form as follows:

$$\alpha = \alpha' A_d^{\beta'}. \tag{B7}$$

B2. Floodplain Cross-Section Coefficient α_f

[52] To determine $\alpha_f \sim A_d^{\beta_f'}$, we make use of the following two floodplain relationships [*Dodov and Foufoula-Georgiou*, 2004]:

$$W_f = \psi_3 A_d^{\theta_3}, \tag{B8}$$

$$h_f = \xi h_{bf}, \tag{B9}$$

where ψ_3, θ_3, and ξ are empirical parameters [see *Dodov and Foufoula-Georgiou*, 2005]. Here h_{bf} [L] is bankfull depth and is given by

$$h_{\mathrm{bf}} = \psi_4 A_d^{\theta_4}. \tag{B10}$$

Solving for α_f in the simplified floodplain power law (i.e., $W_f = \alpha_f h_f^{\beta_f}$) and inserting (B8), (B9), and (B10), we arrive at

$$\alpha_f = \psi_3 (\xi \psi_4)^{-\beta_f} A_d^{\theta_3 - \theta_4 \beta_f}. \tag{B11}$$

In compact form we write (B11) as

$$\alpha_f = \alpha_f' A_d^{\beta_f'}. \tag{B12}$$

Appendix C: Network Hydrodynamic Parameters

C1. Network Celerity

[53] The local celerity u_l [$L\ T^{-1}$] is given by

$$u_l = \frac{\mathrm{d}Q}{\mathrm{d}A}. \tag{C1}$$

Using $A \sim Q^{f'+b'}$ and (C1), we obtain an expression for u_l^{-1}. Then, (B2), (B3), and (B7) are substituted into u_l^{-1}; after inversion, we arrive at

$$u_l = \frac{1}{f'(1+\beta)^{f'\left(1+\frac{5}{3}\beta\right)+m'}} \left[\frac{1}{(\alpha')^2} \left(\frac{\Omega^{1/2}}{\lambda} \right)^{3(1+\beta)} \right]^{\frac{m'}{2}} \cdot A_d^{m'\left[\frac{3}{2}(1+\beta)\left(\frac{\omega}{2}-\tau\right)-\beta'\right]} Q^{m'}. \tag{C2}$$

In compact form we write (C2) as

$$u_l = p A_d^{q'} Q^{m'}. \tag{C3}$$

For the channel, the exponent q' can be simplified to $\theta_2(1-m') - \theta_1$. We assume equilibrium conditions for Q (i.e., $Q = i_e A_d$) to include the dependence of u_l on effective rainfall [*Wang et al.*, 1981; *Rodriguez-Iturbe et al.*, 1982; *Robinson et al.*, 1995]. To obtain a network value for the celerity, a similar harmonic average as given by *Robinson et al.* [1995] is performed. The harmonic average is performed once, as this was found to match more closely the numerical average based on the area function. After the averaging, the network celerity is given by

$$u_n = \left[1 - \frac{(q'+m')}{\phi_3} \right] p A_d^{q'+m'} i_e^{m'}. \tag{C4}$$

To write (C4) in compact form, we just let the coefficient term be equal to p'. Here ϕ_3 enters (C4) as part of the averaging; ϕ_3 is the exponent obtained from the scaling of the mainstream length (i.e., $L_{\mathrm{m}} \sim A_d^{\phi_3}$).

[54] A similar approach is followed to obtain u_n for a floodplain cross section. For the floodplain, the parameters

β, α', and β' in (C2) are simply replaced by β_f, α'_f, and β'_f, respectively.

C2. Network Hydrodynamic Dispersion

[55] The local dispersion D_l [L^2 T^{-1}] is given by

$$D_l = \frac{Q}{2Ws_o}. \tag{C5}$$

By substituting (A3), (B3), and (B7) into (C5), we arrive at

$$D_l = \frac{1}{2}\left[\frac{(1+\beta)^{-\beta}(\alpha')^{-1}}{\Omega^{\frac{10+3\beta}{10}}\lambda^{\frac{3}{5}\beta}}\right]^{f'+m'} A_d^{f'\left[-\frac{5}{3}\beta'-\frac{\omega}{6}(10+3\beta)-\beta\tau\right]} Q^{f'+m'}. \tag{C6}$$

In compact form we write (C6) as

$$D_l = rA_d^{s'}Q^{f'+m'}. \tag{C7}$$

Under equilibrium conditions and performing an arithmetic average [see *Robinson et al.*, 1995], the network hydrodynamic dispersion is given by

$$D_d = \left[1+\frac{(s'+f'+m')}{\phi_3}\right]^{-1} rA_d^{s'+f'+m'} i_e^{f'+m'}. \tag{C8}$$

To write (C8) in compact form we just let the coefficient term be equal to r'. To account for the floodplain geometry in the network hydrodynamic dispersion, we can replace β, α', and β' in (C6) by β_f, α'_f, and β'_f, respectively.

[56] **Acknowledgments.** This research was performed while the first author held a National Research Council Research Associateship Award at the Hydrology Laboratory of NWS, NOAA. We thank the editors and the reviewers for their valuable comments, criticisms, and suggestions.

References

Bhowmik, N. G. (1984), Hydraulic geometry of floodplains, *J. Hydrol.*, *68*(1–4), 369–374, doi:10.1016/0022-1694(84)90221-X.

Bhowmik, N. G., and M. Demissie (1982), Carrying capacity of floodplains, *J. Hydraul. Eng.*, *108*(3), 443–452.

Botter, G., and A. Rinaldo (2003), Scale effect on geomorphologic and kinematic dispersion, *Water Resour. Res.*, *39*(10), 1286, doi:10.1029/2003WR002154.

Buehler, B. (1983), Discussion of "Carrying capacity of flood plains" by Nani Bhowmik and Misganaw Demissie, *J. Hydraul. Eng.*, *109*(4), 643–644, doi:10.1061/(ASCE)0733-9429(1983)109:4(643).

Camporese, M., C. Paniconi, M. Putti, and S. Orlandini (2010), Surface-subsurface flow modeling with path-based runoff routing, boundary condition-based coupling, and assimilation of multisource observation data, *Water Resour. Res.*, *46*, W02512, doi:10.1029/2008WR007536.

Dingman, S. L. (2007), Analytical derivation of at-a-station hydraulic-geometry relations, *J. Hydrol.*, *334*(1–2), 17–27, doi:10.1016/j.jhydrol.2006.09.021.

D'Odorico, P., and R. Rigon (2003), Hillslope and channel contributions to the hydrologic response, *Water Resour. Res.*, *39*(5), 1113, doi:10.1029/2002WR001708.

Dodov, B., and E. Foufoula-Georgiou (2004), Generalized hydraulic geometry: Derivation based on a multiscaling formalism, *Water Resour. Res.*, *40*, W06302, doi:10.1029/2003WR002082.

Dodov, B., and E. Foufoula-Georgiou (2005), Fluvial processes and streamflow variability: Interplay in the scale-frequency continuum and implications for scaling, *Water Resour. Res.*, *41*, W05005, doi:10.1029/2004WR003408.

Dutnell, R. C. (2000), Development of bankfull discharge and channel geometry relationships for natural channel design in Oklahoma using a fluvial geomorphic approach, M.S. thesis, Univ. of Okla., Norman.

Fread, D. L. (1993), Flow routing, in *Handbook of Hydrology*, edited by D. R. Maidment, chap. 10, pp. 10.1–10.36, McGraw-Hill, New York.

Fread, D. L., and J. M. Lewis (1986), Parameter optimization for dynamic flood-routing applications with minimal cross-sectional data, paper presented at ASCE Water Forum '86: World Water Issues in Evolution, Am. Soc. of Civ. Eng., Long Beach, Calif.

Garbrecht, J. (1990), Analytical representation of cross-section hydraulic properties, *J. Hydrol.*, *119*(1–4), 43–56, doi:10.1016/0022-1694(90)90033-T.

Gregory, K. J. (2006), The human role in changing river channels, *Geomorphology*, *79*(3–4), 172–191, doi:10.1016/j.geomorph.2006.06.018.

Hammer, T. (1972), Stream channel enlargement due to urbanization, *Water Resour. Res.*, *8*(6), 1530–1540, doi:10.1029/WR008i006p01530.

Henderson, F. M. (1966), *Open Channel Flow*, Prentice Hall, New York.

Jowett, I. G. (1998), Hydraulic geometry of New Zealand rivers and its use as a preliminary method of habitat assessment, *Regul. Rivers Res. Manage.*, *14*, 451–466.

Kennedy, E. J. (1984), Discharge ratings at gaging stations, *U.S. Geol. Surv. Tech. Water Resour. Invest., Book 3, Chap. A10*, 59 pp.

Knight, D. W., and J. D. Demetriou (1983), Flood plain and main channel flow interaction, *J. Hydraul. Eng.*, *109*(8), 1073–1092, doi:10.1061/(ASCE)0733-9429(1983)109:8(1073).

Kolberg, F., and A. Howard (1995), Active channel geometry and discharge relations of U.S. Piedmont and Midwestern streams: The variable exponent model revisited, *Water Resour. Res.*, *31*(9), 2353–2365, doi:10.1029/95WR01348.

Koren, V., S. Reed, M. Smith, Z. Zhang, and D.-J. Seo (2004), Hydrology laboratory research modeling system (HL-RMS) of the US National Weather Service, *J. Hydrol.*, *291*(3–4), 297–318, doi:10.1016/j.jhydrol.2003.12.039.

Leopold, L. B., and T. Maddock (1953), The hydraulic geometry of stream channels and some physiographic implications, *U.S. Geol. Surv. Prof. Pap.*, *252*.

Leopold, L. B., R. Huppman, and A. Miller (2005), Geomorphic effects of urbanization in forty-one years of observation, *Proc. Am. Philos. Soc.*, *149*(3), 349–371.

Mantilla, R., V. K. Gupta, and O. J. Mesa (2006), Role of coupled flow dynamics and real network structures on Hortonian scaling of peak flows, *J. Hydrol.*, *322*(1–4), 155–167, doi:10.1016/j.jhydrol.2005.03.022.

Mesa, O. J., and E. R. Mifflin (1986), On the relative role of hillslope and network hydraulic geometry in hydrologic response, in *Scale Problems in Hydrology*, edited by V. K. Gupta, I. Rodriguez-Iturbe, and E. F. Wood, pp. 1–17, D. Reidel, Norwell, Mass.

Miller, T. K. (1984), A system model of stream-channel shape and size, *Geol. Soc. Am. Bull.*, *95*(2), 237–241, doi:10.1130/0016-7606(1984)95<237:ASMOSS>2.0.CO;2.

Miller, T. K., and L. J. Onesti (1979), The relationship between channel shape and sediment characteristics in the channel perimeter, *Geol. Soc. Am. Bull.*, *90*(3), 301–304, doi:10.1130/0016-7606(1979)90<301:TRBCSA>2.0.CO;2.

Molnár, P., and J. A. Ramírez (1998), Energy dissipation theories and optimal channel characteristics of river networks, *Water Resour. Res.*, *34*(7), 1809–1818, doi:10.1029/98WR00983.

Myers, W. R. C. (1987), Velocity and discharge in compound channels, *J. Hydraul. Eng.*, *113*(6), 753–766, doi:10.1061/(ASCE)0733-9429(1987)113:6(753).

Myers, W. R. C. (1991), Influence of geometry on discharge capacity of open channels, *J. Hydraul. Eng.*, *117*(5), 676–680, doi:10.1061/(ASCE)0733-9429(1991)117:5(676).

Muneepeerakul, R., A. Rinaldo, and I. Rodriguez-Iturbe (2007), Effects of river flow scaling properties on riparian width and vegetation biomass, *Water Resour. Res.*, *43*, W12406, doi:10.1029/2007WR006100.

Nardi, F., E. R. Vivoni, and S. Grimaldi (2006), Investigating a floodplain scaling relation using a hydrogeomorphic delineation method, *Water Resour. Res.*, *42*, W09409, doi:10.1029/2005WR004155.

Orlandini, S. (2002), On the spatial variation of resistance to flow in upland channel networks, *Water Resour. Res.*, *38*(10), 1197, doi:10.1029/2001WR001187.

Orlandini, S., and R. Rosso (1998), Parameterization of stream channel geometry in the distributed modeling of catchment dynamics, *Water Resour. Res.*, *34*, 1971–1985, doi:10.1029/98WR00257.

Osterkamp, W. R., L. J. Lane, and G. R. Foster (1983), An analytical treatment of channel-morphology relations, *U.S. Geol. Surv. Prof. Pap.*, *1288*.

Paik, K., and P. Kumar (2004), Hydraulic geometry and the nonlinearity of the network instantaneous response, *Water Resour. Res.*, *40*, W03602, doi:10.1029/2003WR002821.

Ponce, V. M., and P. J. Porras (1995), Effect of cross-sectional shape on free-surface instability, *J. Hydraul. Eng.*, *121*(4), 376–380, doi:10.1061/(ASCE)0733-9429(1995)121:4(376).

Reed, S., J. Schaake, and Z. Zhang (2007), A distributed hydrologic model and threshold frequency-based method for flash flood forecasting at ungauged locations, *J. Hydrol.*, *337*(3–4), 402–420, doi:10.1016/j.jhydrol.2007.02.015.

Rhoads, B. (1991), A continuously varying parameter model of downstream hydraulic geometry, *Water Resour. Res.*, *27*(8), 1865–1872, doi:10.1029/91WR01363.

Rinaldo, A., A. Marani, and R. Rigon (1991), Geomorphological dispersion, *Water Resour. Res.*, *27*(4), 513–525, doi:10.1029/90WR02501.

Rinaldo, A., G. Vogel, R. Rigon, and I. Rodriguez-Iturbe (1995), Can one gauge the shape of a basin?, *Water Resour. Res.*, *31*(4), 1119–1127, doi:10.1029/94WR03290.

Robinson, J. S., M. Sivapalan, and J. D. Snell (1995), On the relative roles of hillslope processes, channel routing, and network geomorphology in the hydrologic response of natural catchments, *Water Resour. Res.*, *31*(12), 3089–3101, doi:10.1029/95WR01948.

Rodriguez-Iturbe, I., and A. Rinaldo (Eds.) (1997), *Fractal River Basins: Chance and Self-Organization*, Cambridge Univ. Press, New York.

Rodriguez-Iturbe, I., and J. Valdés (1979), The geomorphologic structure of hydrologic response, *Water Resour. Res.*, *15*(6), 1409–1420, doi:10.1029/WR015i006p01409.

Rodriguez-Iturbe, I., M. González-Sanabria, and R. Bras (1982), A geomorphoclimatic theory of the instantaneous unit hydrograph, *Water Resour. Res.*, *18*(4), 877–886, doi:10.1029/WR018i004p00877.

Saco, P. M., and P. Kumar (2002a), Kinematic dispersion in stream networks: 1. Coupling hydraulic and network geometry, *Water Resour. Res.*, *38*(11), 1244, doi:10.1029/2001WR000695.

Saco, P. M., and P. Kumar (2002b), Kinematic dispersion in stream networks: 2. Scale issues and self-similar network organization, *Water Resour. Res.*, *38*(11), 1245, doi:10.1029/2001WR000694.

Saco, P. M., and P. Kumar (2004), Kinematic dispersion effects of hillslope velocities, *Water Resour. Res.*, *40*, W01301, doi:10.1029/2003WR002024.

Schumm, S. A. (1960), The shape of alluvial channels in relation to sediment type, *U.S. Geol. Surv. Prof. Pap.*, *352B*.

Singh, V. P. (1996), *Kinematic Wave Modeling in Water Resources: Surface Water Hydrology*, John Wiley, New York.

Smith, L. C., and T. M. Pavelsky (2008), Estimation of river discharge, propagation speed, and hydraulic geometry from space: Lena River, Siberia, *Water Resour. Res.*, *44*, W03427, doi:10.1029/2007WR006133.

Smith, M. B., D.-J. Seo, V. Koren, S. M. Reed, Z. Zhang, Q. Duan, F. Moreda, and S. Cong (2004), The distributed model intercomparison project (DMIP): Motivation and experiment design, *J. Hydrol.*, *298*(1–4), 4–26, doi:10.1016/j.jhydrol.2004.03.040.

Snell, J. D., and M. Sivapalan (1994), On geomorphological dispersion in natural catchments and the geomorphological unit hydrograph, *Water Resour. Res.*, *30*(7), 2311–2323, doi:10.1029/94WR00537.

Sturm, T. (2001), *Open Channel Hydraulics*, McGraw-Hill, New York.

Tarboton, D. G., R. L. Bras, and I. Rodriguez-Iturbe (1989), Scaling and elevation in river networks, *Water Resour. Res.*, *25*(9), 2037–2051, doi:10.1029/WR025i009p02037.

Tortorelli, R. L. (1997), Techniques for estimating peak-streamflow frequency for unregulated streams and streams regulated by small floodwater-retarding structures in Oklahoma, *U.S. Geol. Surv. Water Resour. Invest. Rep. 97-4202*.

Valiani, A., and V. Caleffi (2009). Analytical findings for power law cross-sections: Uniform flow depth, *Adv. Water Resour.*, *32*(9), 1404–1412, doi:10.1016/j.advwatres.2009.06.004.

van der Tak, L. D., and R. L. Bras (1990), Incorporating hillslope effects into the geomorphological instantaneous unit hydrograph, *Water Resour. Res.*, *26*(10), 2393–2400, doi:10.1029/WR026i010p02393.

Wang, C. T., V. K. Gupta, and E. Waymire (1981), A geomorphologic synthesis of nonlinearity in surface runoff, *Water Resour. Res.*, *17*(3), 545–554, doi:10.1029/WR017i003p00545.

Western, A. W., B. L. Finlayson, T. A. McMahon, and I. C. O'Neill (1997), A method for characterising longitudinal irregularity in river channels, *Geomorphology*, *21*(1), 39–51, doi:10.1016/S0169-555X(97)00023-8.

Wilcock, D. N. (1971), Investigation into the relations between bedload transport and channel shape, *Geol. Soc. Am. Bull.*, *82*(8), 2159–2176, doi:10.1130/0016-7606(1971)82[2159:IITRBB]2.0.CO;2.

Woltemade, C., and K. Potter (1994), A watershed modeling analysis of fluvial geomorphologic influences on flood peak attenuation, *Water Resour. Res.*, *30*(6), 1933–1942, doi:10.1029/94WR00323.

A. I. Mejia and S. M. Reed, Office of Hydrologic Development, National Weather Service, NOAA, 1325 East-West Hwy., Silver Spring, MD 20910, USA. (alfonso.mejia@noaa.gov)